Chapter 2

ANALYSIS OF ON-AXIS HOLOGRAPHY WITH FEMTOSECOND PULSES

2.1 CAPTURE OF NONLINEAR PULSE PROPAGATION WITH PULSED-HOLOGRAPHY

Very high intensity levels can be achieved with femtosecond pulses due to their short time duration. Ultrashort pulses can significantly change the properties of the medium through which they propagate, which in turn alters the pulse itself. Much can be learned about the propagation of pulses from the changes in the material properties. The time scale of the changes ranges from instantaneous to permanent. Ultrafast nonlinear index changes can be as fast as a femtosecond or last for several picoseconds. Plasma generated through ionization of the material has a lifetime on the order of nanoseconds, while index changes due to heating can last for milliseconds. There can also be a permanent effect on the material, such as in the case of laser ablation or permanent index changes due to melting. Pulsed holography provides an ideal way to observe these index changes. The index changes can be reconstructed from the phase information in the hologram, while the duration of the pulse provides time resolution to focus on the time window of interest. We have used an on-axis [1] holographic setup, in which a femtosecond probe pulse captures the changes in the material properties. The holographic camera records either a single hologram with high spatial resolution (4μm) or a time-sequence of four holograms (holographic movie) with reduced spatial resolution. The main advantage of using on-axis holography is that there is no need for reference pulses, as both the signal and reference are generated from a single probe pulse. The holograms are recorded on a CCD camera and reconstructed numerically [2-4]. Multiple holograms can be captured on a single frame of

the CCD camera by spatially separating them (spatial multiplexing). With the multiple frame capture, the time evolution of the pulse propagation is captured in a single-shot experiment.

In this chapter we briefly discuss the sources of nonlinear index changes that can be observed with femtosecond pulses. The Kerr effect (third order optical nonlinearity) generates a positive index change with a femtosecond to picosecond duration. Ionization of the medium (plasma formation) results in a negative index change with a lifetime on the order of nanoseconds. The changes in the material properties are captured by a weak probe pulse, which temporally and spatially overlaps with a strong pump pulse. The short duration of the pulses plays a major role in the overlap and interaction of the pulses. The interaction can be analyzed using some simple geometrical arguments. The main limitation of on-axis holography is the appearance of twin images when the hologram is reconstructed. The reconstruction is distorted by the appearance of a defocused virtual image along with the real image. We will discuss how this affects the accuracy of our measurements and present an iterative algorithm to remove the effect of the twin image. Finally we discuss the coupling between spatial and temporal resolution limits of on-axis holograms. The following chapter describes the holographic camera in detail and the results for pulse propagation through different materials.

2.2 INDUCED NONLINEAR INDEX CHANGES

2.2.1. Kerr effect

The advantage of the holographic recording is that it captures the index changes due to both the Kerr nonlinearty (in general positive) and plasma generation (negative index change), along with changes in the amount of light transmitted by the material. When the intensity of the incident light is very high, the nonlinear contributions to the polarization of the medium must be taken into account. If the electric due to the incident light is small compared to the atomic electric field, the polarization can be expanded in a power series:

$$P_i = \chi_{ij}^{(1)} E_j + \chi_{ijk}^{(2)} E_j E_k + \chi_{ijkm}^{(3)} E_j E_k E_m + \ldots, \tag{2.1}$$

where $\chi^{(n)}$ is a tensor of order $(n+1)$ that represents the n^{th} order response of the material and P_i and E_i are the i^{th} vector components of the polarization and the electric field, respectively. The three terms on the right hand side are the linear response of the material, the second order nonlinear response and the third order nonlinearity, respectively. The nonlinear terms can generate a polarization at frequencies different from that of the incident light, for example, the second order term is responsible for second harmonic generation. It is known that for isotropic materials the second order response vanishes [5]. The term responsible for a self-induced nonlinear index change in the material is the third order response:

$$P^{NL} = \chi^{(3)} |E|^2 E\,. \tag{2.2}$$

This is commonly referred to as the Kerr effect. The response of the material is proportional to the square of the electric field. This can also be written as an index of refraction with a linear contribution, which is constant, and a nonlinear contribution that depends on the intensity of the light [6]:

$$n = n_0 + n_2 I\,, \tag{2.3}$$

where n_0 is the refractive index of the material, n_2 is the Kerr coefficient of the material and I is the light intensity. The Kerr coefficient can be positive or negative, and depends on the duration of the incident light and the frequency. For CW light or long laser pulses (microseconds) the thermal response of the material dominates resulting in a negative n_2. The heating of the material causes a density change and a negative index change. If the material is studied with ultra-short pulses, on the order of tens of picoseconds or shorter, the excitation is too short for thermal effects to play a role. In this case the main contributions are the instantaneous electronic response of the material (with a time constant of the order of a femtosecond) and the molecular response (with time constants on the order of picoseconds). The instantaneous response corresponds to the electronic response in the atom or molecule to the incident electric field, while the molecular response corresponds to

excitation of the molecules (vibration, rotation, etc.). The ultra-fast Kerr effect is positive for most material, although some exceptions have been found in some special polymers [7]. For any given material, then, the strength and sign of the Kerr effect that is observed will depend on the duration of the incident laser pulses. For excitation with 150-femtosecond pulses, it is possible to observe both electronic and molecular responses, although the electronic response dominates in general.

A positive Kerr response means that a non-uniform laser beam will experience self-focusing. For example, a beam with a Gaussian spatial profile will have a higher intensity at the center of the beam. There will be an index change in the material that is higher near the center of the beam and vanishes at the edge of the beam. This index change will act as a lens and focus the beam. A laser pulse will experience self-focusing if its power is higher than a critical value, defined as [5]:

$$P_{cr} = \frac{\pi(0.61)^2 \lambda^2}{8 n_0 n_2}, \tag{2.4}$$

where λ is the laser wavelength. At the critical power, the nonlinearity exactly cancels the effect of diffraction; the beam becomes self-trapped and propagates with a constant diameter. This is, however, an unstable equilibrium. If the power is initially below the critical value the beam will diffract, and if the power is above the critical value the beam will continue to self-focus until another mechanism acts to balance the self focusing. This balancing can lead to the formation of optical spatial solitons and will be discussed in detail in the following chapters. When the power of the pulses is much greater than the critical power ($P > 100\ P_{cr}$) the beam will break up into multiple filaments, each one carrying approximately the critical power. Any initial modulation (noise) in the input beam will be amplified by the self focusing process, eventually resulting in the beam breaking up into smaller beams, or filaments (Fig. 2.1).

2.2.2. Index change due to plasma generation

If the intensity of the filaments exceeds the breakdown threshold of the material, free electrons are generated. For excitation with ultrashort (femtosecond) pulses, the dominant mechanism for plasma formation is multi-photon absorption. A single electron will absorb multiple photons at the same time, and the medium becomes ionized. The plasma generated induces a negative index change, which can balance the positive index change of the Kerr effect. The plasma index change is given by:

$$\Delta n = \sqrt{1 - \frac{\omega_p^2}{\omega}} - 1 \approx \frac{-\omega_p^2}{2\omega^2}, \tag{2.5}$$

where ω = 2.36 x 10^{15} s^{-1} is the angular frequency of the laser and ω_p is the plasma frequency:

$$\omega_p^2 = \frac{Ne^2}{\varepsilon_0 m}, \tag{2.6}$$

where N is the electron density, e = 1.6 x 10^{-19} C is the charge of the electron, m = 9.1 x 10^{-31} kg is the mass of the electron and ε_0 = 8.85 x 10^{-12} $C^2s^2m^{-3}kg^{-1}$ is the permittivity of free space. The plasma density can thus be calculated if the index change is measured. The plasma index change can stabilize the self-focusing due to the Kerr effect [8, 9]. As the filaments continue to focus and the intensity increases, the plasma density and negative index change also increase. Eventually the negative index change becomes strong enough so as to defocus the light, at which point the intensity and plasma density decrease, leading to a new cycle of self focusing. Some energy is lost through the ionization process, so eventually the cycle stops when the power in the beam is no longer above the critical power. In the absence of plasma, a higher nonlinearity (fifth order nonlinearity) can act to balance the self-focusing through a saturation of the index change [10]. Which effect becomes dominant depends on the material properties and the intensity and duration of the pulses.

2.3 INTERACTION AND OVERLAP OF FEMTOSECOND PULSES

The holographic recording technique uses a strong pump pulse that interacts with the material and a weak probe pulse that captures the changes in the material. Any instantaneous changes in the material properties will be captured only when the pump and probe overlap temporally and spatially. Long-lasting changes in the material, lasting longer than a few hundred femtoseconds, can also be observed after the pump pulse has traversed the material. The instantaneous changes will reveal a snapshot of the pump pulse traversing the material, while the long lasting changes will appear as a trail behind the moving pulse. The trail can be due to the delayed Kerr response, with a time constant of picoseconds, or a plasma trail that lasts for a longer time (nanoseconds). The probe pulses, which propagate at an angle relative to the pump, are captured using a CCD camera (Fig. 2.1).

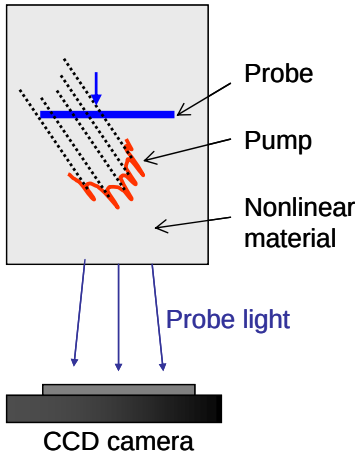

Figure 2.1. Sketch of holographic capture. There are an instantaneous component of the index change and a trail behind the pulse that contribute to the signal on the probe pulse. The probe light is captured on a CCD camera.

The angle difference between pump and probe is in the horizontal direction, as observed on the camera. Smaller angles lead to longer interaction lengths and increased signal strength as the phase changes in the probe accumulate over a longer distance. If the pump pulse

leaves a trail in the material that lasts longer than the time window of the experiment (a few picoseconds), then a probe arriving after the pump will capture the entire trail. An instantaneous effect, however, can only be captured when the pulses overlap temporally and spatially. For two ultrashort pulses propagating at an angle, the overlap region will be a thin strip at the midline between the two pulses (Fig. 2.2). The width of the overlap strip depends on the duration of the pulses and the angle between them:

$$w_o = \frac{c\tau}{n\sin(\theta/2)} A_t = \frac{w_t}{\sin(\theta/2)} A_t , \tag{2.7}$$

where τ is the duration of the pulses, θ is the angle between the two beams inside the medium, c is the speed of light, n is the index of refraction, A_t is a numerical factor that depends on the shape of the temporal envelope of the pulses and w_t is the length of the pulses in space. The temporal profile of the pulses is approximately Gaussian, in which case $A_t = 0.707$.

The total length of the overlap region is

$$L_o = \frac{D}{\sin(\theta/2)} A_s , \tag{2.8}$$

where D is the diameter of the smaller (pump) beam, and A_s is a numerical factor that depends on the shape of the spatial beam profile. As observed on the CCD camera, the signal width in the horizontal direction will be a projection of both the width and the length of the overlap region. The size of the overlap region projected on the CCD camera can be approximated as:

$$L_{CCD} \approx DA_s + \frac{w_t}{\tan(\theta/2)} A_t . \tag{2.9}$$

The first term dominates for large beam diameter, while the second term becomes important for small beam diameters and small angles. The signal width on the CCD along the vertical direction will be equal to the pump beam diameter D.

If the time delay of the probe is changed the pulses will overlap at a different position, resulting in the motion of the pump pulse on the camera. The velocity of the pulse inside the medium can be calculated from the apparent velocity of the pulse on the camera:

$$v = \frac{\Delta x}{\Delta t}\tan(\theta/2), \tag{2.10}$$

where Δx is the change in position of the pump in the camera, and Δt is the time delay. For a 90-degree setup there is a one-to-one correspondence between the apparent and real speeds.

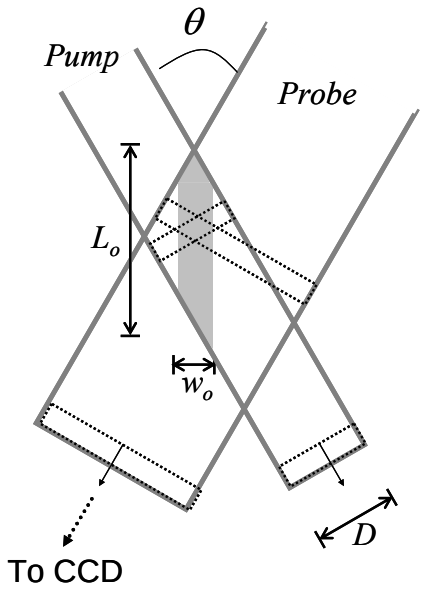

Figure 2.2. Overlap region for two ultrashort pulses. The overlap region is a thin strip along the center line between the two pulses. The width of the strip is determined by the duration of the pulses, while the length of the strip is determined by the beam size.

2.4. DIGITAL RECORDING AND RECONSTRUCTION OF ON-AXIS HOLOGRAMS

2.4.1. On-axis holograms and the twin image problem

The use of on-axis (self-referenced) holograms allows us to record holograms without having to separately generate a sequence of signal and reference pulses. The object is illuminated by a plane wave and the light scattered by the object interferes with the transmitted light (Fig. 2.3a). The intensity of the light field at the recording plane is captured with a CCD camera, which allows us to reconstruct the hologram numerically on the computer. Accurate holographic reconstructions can be obtained provided the amount of light scattered by the object is small compared to the transmitted light.

The object is illuminated by a plane wave, which we normalize to be of unit amplitude. The complex light field at the object plane is:

$$F_O(x,y) = 1 + O(x,y)\,. \tag{2.11}$$

O(x,y) is the complex disturbance of the light field induced by the object. We assume that the area covered by the object is small compared to the area of the illuminating beam (or the area of the camera, whichever is smallest). This ensures that at the detector the transmitted light field will be much stronger than the object field.

The field at the hologram plane, a distance z from the object plane, is obtained by convolving the object field with the Fresnel convolution kernel [11]:

$$F_H(x,y) = \left[1 + O(x,y)\right] \otimes h_z(x,y)\,, \tag{2.12}$$

where $h_z(x,y)$ is the Fresnel convolution kernel:

$$h_z(x,y) = \frac{Exp(jkz)}{j\lambda z} Exp\left[\frac{jk}{2z}\left(x^2 + y^2\right)\right]. \tag{2.13}$$

The convolution can be calculated on the computer using Fast Fourier Transforms. If F_H *(x,y)* is known, the object field can be reconstructed exactly applying the Fresnel convolution kernel in the opposite direction (-*z*). However, the hologram captures only the intensity of the light at the hologram plane:

$$H(x,y) = \left|F_H(x,y)\right|^2 = \left|\left[1 + O(x,y)\right] \otimes h_z(x,y)\right|^2 . \tag{2.14}$$

If we now try to reconstruct the object field from the intensity measurement using the Fresnel convolution kernel, the reconstructed field contains the desired object field plus an extra term:

$$F_R(x,y) = H(x,y) \otimes h_{-z}(x,y) = 1 + O(x,y) + O^*(x,y) \otimes h_{-2z}(x,y) . \tag{2.15}$$

The first term on the right-hand side represents the transmitted light (plane wave). The second term is the object field and the third term is a twin image, which is the conjugate of the object field diffracted by a distance of -2*z*. A term of order square of the object field was neglected. The holographic reconstruction contains the desired amplitude and phase information, but is distorted by the presence of the twin image (Fig. 2.3b) [1, 12]. For small objects, the distortion will in most cases appear in the form of fringes around the object. The twin image problem is caused by the loss of the phase information when the hologram is recorded (the camera captures only the intensity of the light field). The twin image is present in both optically and digitally reconstructed on-axis holograms. The problem is less severe for small objects and large recording distance *z*, in which case the twin image will appear as background noise around the true object.

The digital holograms also contain 3-D information about the object. The hologram can be numerically re-focused at different planes by changing the distance *z* in the Fresnel kernel (equation 2.13), bringing different object features to focus and revealing three-dimensional structure. We will show an example of this in the next chapter.

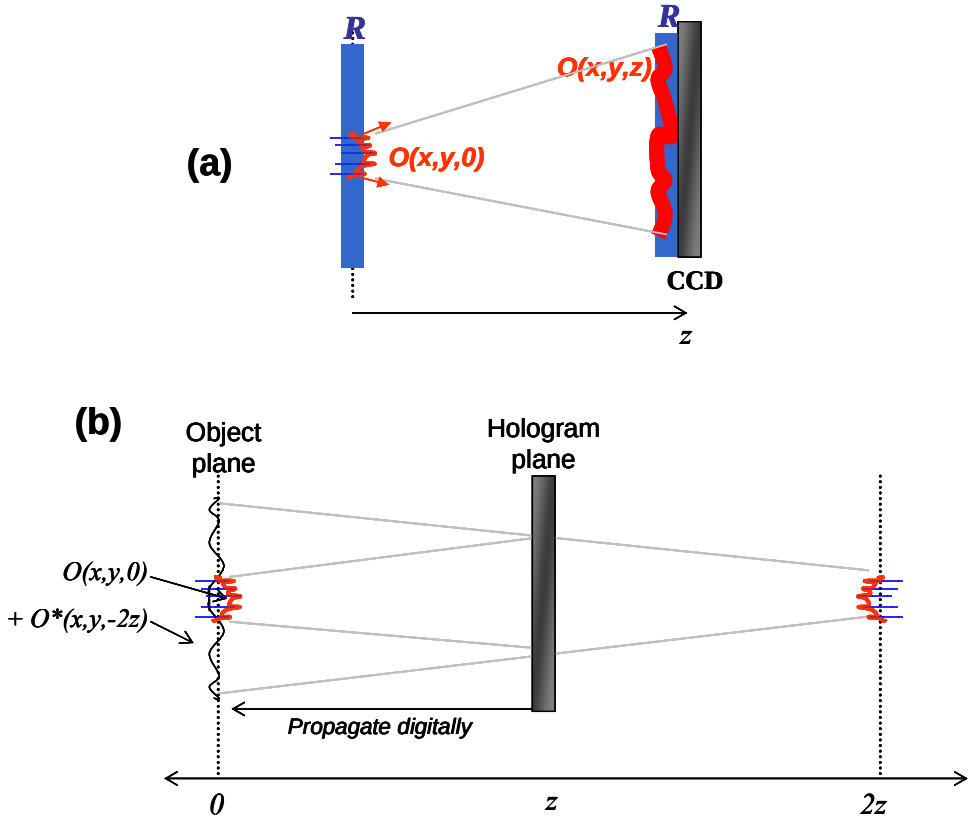

Figure 2.3. Recording and reconstruction of on-axis holograms. (a) Recording geometry. (b) Both a real and a virtual image appear in the reconstruction.

2.4.2. Numerical reconstruction for small objects

In our experimental setup for single frame capture, the distortion due to the twin image does not significantly affect accuracy of the reconstruction. The pump pulse breaks up into small filaments with a diameter of 4 μm to 15 μm and lengths of approximately 1 mm. After a magnification factor of 12 a filament covers only a small fraction of the recording area (the CCD sensor area is 14.8 mm x 10.2 mm).

We have performed numerical simulations to calculate the distortion induced by the presence of the twin image. The diffraction pattern due to a filament with a diameter of 8

μm and a length of 500 μm was calculated for a recording distance of 25 cm. The accumulated phase change for a beam that traverses the filament is 1 rad, caused by an index change in the material. The magnification, pixel size and number of pixels are the same as in the experimental apparatus (M = 12, 2184 x 1472 pixels, 6.8 μm pixel size). The phase change and filament size are comparable to those observed experimentally for plasma filaments generated in air, as described in the following sections (with the difference that the plasma generates a negative index change). The light propagation from the object plane to the recording plane is calculated numerically using the Fresnel convolution Kernel (equations 2.12-13). The intensity pattern at the recording plane is used to calculate the reconstruction at the object plane. Figure 2.4a shows a cross section of the phase of the input and reconstructed light field. The reconstruction agrees very well with the simulated filament at the position of the filament. The maximum phase change and width of the input and reconstructed filaments differs by less than 5%. The inset shows a close-up of the filament region. Outside the filament area the reconstruction shows the fringes characteristic of the twin image. In the experimental images two filaments may appear in close proximity, so we also simulated two filaments with 8 μm diameter separated by 16 μm (Fig. 2.4b). In this case there was also good agreement between the input and the reconstruction, with the characteristic fringes outside of the object area. The error, however, increases rapidly with object size. In the next section we present an iterative technique that can reduce the distortion when the object occupies a larger fraction of the hologram area.

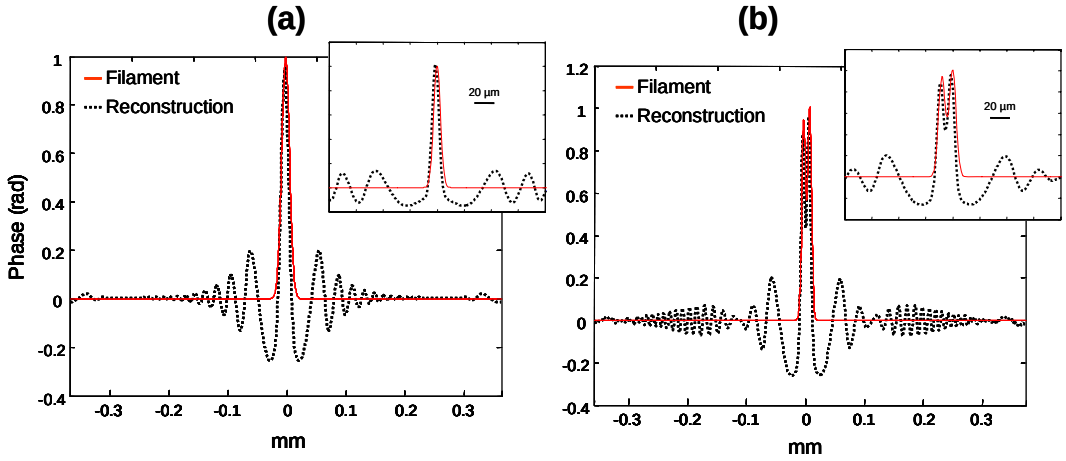

Figure 2.4. Simulation of phase reconstruction from on-axis holograms. a) Cross section of simulated (red, solid line) and reconstructed (black, dotted line) phase filament with 8 μm diameter. b) Simulation and reconstruction of double filament. The insets shows a close-up of the filament and reconstruction. In both cases the reconstruction is accurate at the position of the filament.

2.5. REMOVAL OF THE TWIN IMAGE

As the size of the object relative to the recording area increases, the distortion due to the twin image becomes more severe. In the case when multiple holograms are multiplexed on a single frame of the CCD camera, the distortion can be significant. The twin image can be removed if the phase of the light at the recording plane is recovered. Digital holograms have the advantage that this distortion can be corrected numerically. A number of algorithms have been implemented to recover the phase of the hologram. One method uses a double exposure [13] to calculate the phase from two intensity measurements, while the most common method is to use an iterative algorithm [12, 14, 15]. Iterative techniques in general assume that the object is real, that is, the object affects only the amplitude of the light field. The real part of the initial reconstruction is used as the starting point, and the

reconstruction is iterated applying the constraint that the object reconstruction be real at each step. This method works well for image reconstruction; however, it does not allow one to recover both amplitude and phase.

We have developed a variation of the iterative technique that allows us to reconstruct both amplitude and phase for objects that are small compared to the area of the hologram. The unknown that we need to recover in order to remove the twin image is the phase of the field at the hologram plane. We know that the phase and amplitude of the object reconstruction must be constant outside of the object area, given that it was originally illuminated with a plane wave. The light field that we want to recover is given by equation 2.11. After the initial reconstruction (equation 2.15) it is in general possible to estimate the size and position of the object, even though there is distortion from the presence of the twin image. The object reconstruction will be localized, while the twin image will be spread out due to diffraction. The initial reconstruction F_R is used as the starting point of the iterative reconstruction. A new field is generated by applying the constraint of a plane wave illumination. Specifically, the constraint is applied by multiplying the reconstruction with an aperture function that is unity in the estimated object area and zero outside. The zeroed area is replaced by a uniform field with the mean amplitude and phase of the original field. The initial guess for the iterative algorithm is:

$$\begin{aligned} F_{G1}(x,y) &= A(x,y)F_R(x,y) + \big(1 - A(x,y)\big) \\ &= 1 + A(x,y)O(x,y) + A(x,y)\Big(O^*(x,y) \otimes h_{-2z}(x,y)\Big), \end{aligned} \tag{2.16}$$

where *A(x,y)* is unity inside the estimated object area and zero outside. If the function *A(x,y)* is chosen properly, it will only affect the twin image:

$$F_{G1}(x,y) = 1 + O(x,y) + A(x,y)\Big(O^*(x,y) \otimes h_{-2z}(x,y)\Big). \tag{2.17}$$

The light field at the hologram plane is calculated by numerically propagating the guessed object field F_{G1} by a distance z:

$$\begin{aligned} F_{H1}(x,y) &= F_{G1}(x,y) \otimes h_z(x,y) \\ &= \big[1 + O(x,y)\big] \otimes h_z(x,y) + \Big[A(x,y)\Big(O^*(x,y) \otimes h_{-2z}(x,y)\Big)\Big] \otimes h_z(x,y), \end{aligned} \tag{2.18}$$

where the first term on the second line is what we want to recover, while the second term is due to the twin image. The effect of the aperture function *A(x,y)* is to reduce the strength of the contribution from the twin image at the recording plane. If *A(x,y)* is set to one everywhere, the sum of the contributions from the real and the virtual images results in a real field, and no phase information is recovered. For large recording distance *z*, the aperture function is effectively transmitting only the low frequency components of the twin image, thus reducing the phase modulation due to the twin image at the hologram plane. A corrected field is generated by combining the measured intensity with the reconstructed phase:

$$\overline{F}_{H1}(x,y) = \sqrt{H(x,y)}\exp\left[i * \text{Phase}\left(F_{H1}(x,y)\right)\right], \tag{2.19}$$

where *H(x,y)* is the intensity distribution of the hologram measured on the CCD camera, and Phase($F_{H1}(x,y)$) is the phase of F_{H1}. The corrected field is used to generate a new object reconstruction and start a new cycle:

$$F_{R2}(x,y) = \overline{F}_{H1}(x,y) \otimes h_{-z}(x,y) = \left[1 + O(x,y)\right] + T_1(x,y) \ , \tag{2.20}$$

where $T_1(x,y)$ is the distortion of the field due to the twin image that is left after 1 iteration. A second guess is generated using the same procedure as before:

$$F_{G2}(x,y) = A(x,y)F_{R2}(x,y) + \left(1 - A(x,y)\right) = \left[1 + O(x,y)\right] + A(x,y)T_1(x,y) \, . \tag{2.21}$$

The new guess is used for a new iteration. The function $T_n(x,y)$ will in general get weaker after each iteration. The process continues until the reconstruction no longer changes. The number of iterations depends on the amount of distortion in the initial reconstruction. A stable reconstruction is generally achieved after 4-10 iterations. The performance of the algorithm can be monitored qualitatively by the decrease in the characteristic fringes around the object with each iteration or quantitatively using numerical simulations. It is important to choose the correct size for the aperture function. If the aperture is too small it will distort the reconstruction, as the object will fill the aperture area. If the aperture size is too large then it might not have a strong enough effect on the twin image. The most

efficient method to choose the aperture was to use the phase of the reconstruction to determine the size of the object, and to fine tune the aperture by looking at the results. We have seen that the shape of the aperture is not very critical unless the object is very asymmetric. A simple rectangular aperture has given good results in most cases.

We have numerically tested the algorithm and seen a significant improvement in the accuracy of the reconstructions. The simulation is run for a detector size of 512 pixels by 512 pixels (6.8 μm pixel size), about one fourth of the size of our CCD camera, and no magnification. We simulate an object field with Gaussian shape (width = 0.11 mm, length = 0.44 mm) with a positive phase change and absorption. The peak phase change is 1 radian and the minimum amplitude transmittance is 70 %. These values are similar to those observed in several of the experiments. Figure 2.5 shows the amplitude of (a) the simulated object field, (b) the initial reconstruction and (c) the initial guess used for the iterative technique, while (d-f) shows the phase of the object, the reconstruction and the initial guess, respectively. Figure 2.6 shows the corrected amplitude and phase reconstructions after applying 2, 8 and 20 iterations of the algorithm. After 8 iterations the algorithm reaches a stable point and the reconstruction no longer changes. The minimum transmittance in the initial reconstruction is 87 %, compared to 74 % after the correction (8 iterations), which is closer to the true value of 70%. Similarly, the peak phase change of the initial reconstruction is 0.50 radians and improves to 0.83 radians. The shape of the reconstructed field also improves significantly, note that the amplitude change is much narrower before the reconstruction. Figure 2.7 shows plots of a vertical cross section along the center of the image of the amplitude (Fig. 2.6a) and the phase (Fig. 2.6b) of the simulated object, the initial reconstruction and the corrected reconstruction after 8 iterations. It is clear from these plots that the accuracy of the reconstruction improves significantly and that the ringing due to the twin image is reduced. We have run the simulation for objects of different sizes and different field strengths and seen significant improvement in most cases. Objects with sharp edges are in general easier to correct since they have well-defined boundaries. The reconstructed error depends on the object field and increases with object size. The size of the objects captured in our experiments is in general

smaller than the object used for the simulation, and the algorithm usually converges to a stable solution within 4-10 iterations.

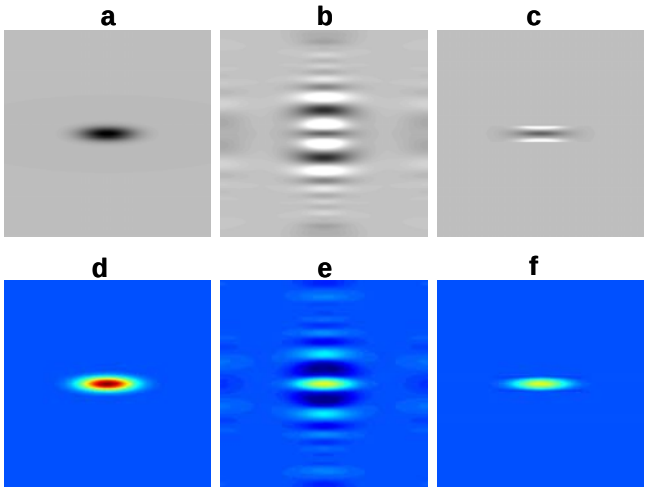

Figure 2.5. Simulation of object reconstruction. (a) Amplitude of simulated object field. (b) Initial amplitude reconstruction. (c) Intial guess for iterative reconstruction algorithm. (d-f) Phase of the light fields in (a-c), respectively. The phase is color coded such that red indicates a high value of the phase and blue corresponds to low values.

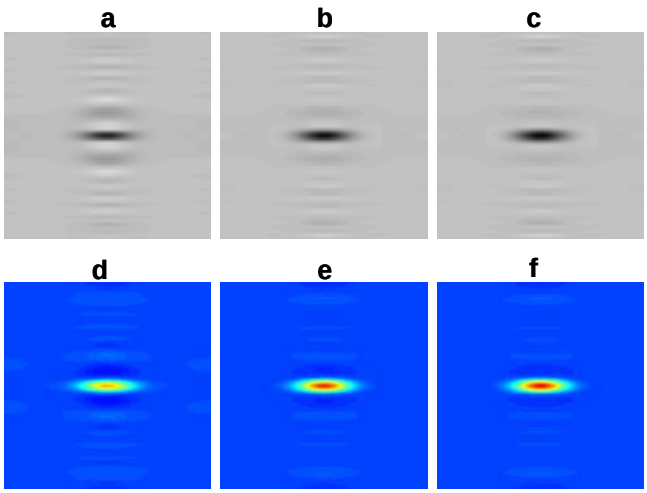

Figure 2.6. Amplitude and phase reconstructions with iterative algorithm. (a-c) Amplitude reconstructions after 2, 8 and 20 iterations. (d-f) Phase reconstruction after 2, 8 and 20 iterations.

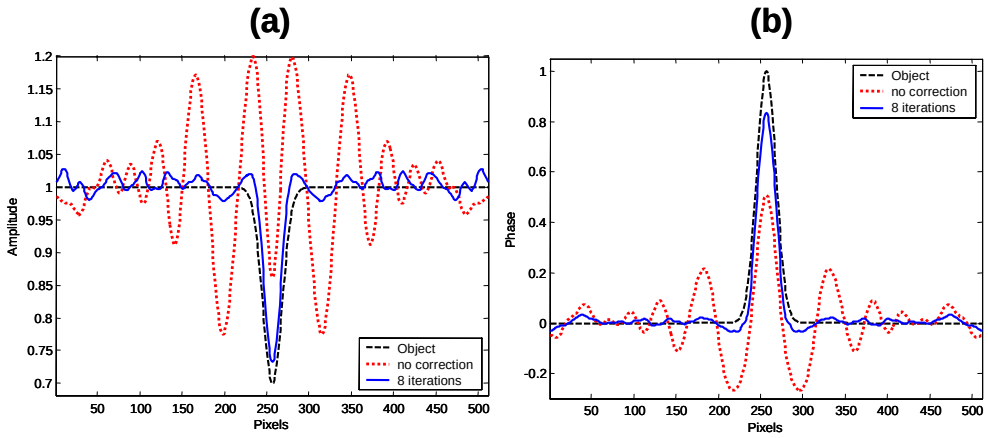

Figure 2.7. Cross sectional plots of simulated object (dashed black line), initial reconstruction (dotted red line) and the reconstruction after applying the correction algorithm (solid blue line). (a) Vertical cross section of the amplitude of the light along the center of the image. (b) Cross section of the phase.

Figure 2.8 shows the results of the correction algorithm when applied to an experimentally recorded hologram of a pulse propagating in water (the experimental results will be discussed in detail in the next chapter). Figure 2.8a shows a hologram recorded using approximately one quarter of the CCD area with the multiple-frame setup. The pump pulse generates an index change in the water, which induces a phase change in the probe pulse. Figure 2.8b-c shows the phase reconstruction before and after applying the correction algorithm (6 iterations). The fringes due to the twin image become much weaker and the detail around the object becomes sharper. Similar improvement was observed for most reconstructions. In the case of high resolution holograms with small filaments the improvement is not as significant since the initial reconstructions are already quite accurate. Finally, if a large phase change is measured it is necessary to unwrap the phase in order to calculate the index changes. Several algorithms have been developed to solve the problem of phase-unwrapping in 2-D. We have obtained good results with the algorithm developed by Volkov and Zhu [16].

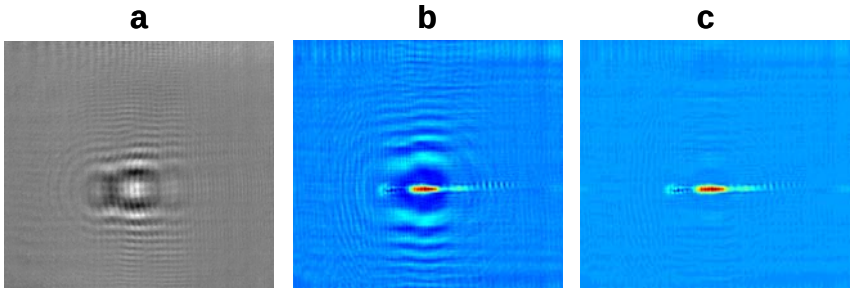

Figure 2.8. Phase reconstruction of an experimentally recorded hologram. (a) Hologram captured on the CCD camera using the movie setup. (b-c) Phase reconstruction before and after applying the correction algorithm. The light pulse propagates from left to right. The image size is 5.0 mm x 5.4 mm.

2.6 RECONSTRUCTION OF INDEX CHANGES

The nonlinear index changes in the material can be recovered from the phase information in the hologram. A probe that traverses a material with an index change will accumulate a phase change that is proportional to the index change in the material:

$$\Delta\phi(x,y) = \frac{2\pi}{\lambda}\int_0^L \Delta n(x,y,z)dz\,, \tag{2.22}$$

where we assume a probe propagating in the *z*-direction, Δn is the index change and L is the length of the index change traversed by the probe. L can be calculated from the beam size and the formulas in section 2.3. The previous formula can be used to reconstruct the index changes averaged over the *z*-direction:

$$\frac{\Delta\phi(x,y)}{2\pi} = \frac{L}{\lambda}\langle\Delta n(x,y)\rangle\,, \tag{2.23}$$

where the term in brackets is the index change averaged in the *z*-direction. This formula can be used to reconstruct the transverse profile of index change from the measured phase changes.

2.7. RESOLUTION LIMITS OF FEMTOSECOND HOLOGRAPHY

The temporal resolution of the holographic reconstruction is limited by the duration of the laser pulses. When recording with CW light or long laser pulses, the spatial resolution of on-axis holograms is determined by the numerical aperture. The minimum resolvable feature is

$$\delta_H = 0.61\frac{\lambda}{NA_H}\,, \tag{2.24}$$

where λ is the laser wavelength and NA_H is the numerical aperture of the hologram:

$$NA_H = \frac{D}{\sqrt{(2z)^2 + D^2}} \approx \frac{D}{2z}, \tag{2.25}$$

D is the detector size and z is the distance from the object to the recording plane (D is in general much smaller than z). In the case of digital holograms the resolution cannot exceed the detector pixel size unless the object is optically magnified. If magnification is used, the resolution will be determined by the smallest between the numerical aperture of the imaging system and numerical aperture of the hologram.

For very short pulses, however, the effect of the short coherence length needs to be taken into account. Consider a short pulse that illuminates a small object (Fig. 2.9a). The transmitted light (reference) is a plane wave, while the scattered light will propagate at a range of angles that depend on the spatial frequencies contained in the object. The time of arrival of the scattered light at the detector depends on the angle of propagation. Light scattered at larger angles (which corresponds to larger spatial frequencies) has to travel a longer distance to arrive at the detector. If the transmitted and scattered pulses do not temporally overlap on the detector they will not interfere, therefore limiting the effective numerical aperture. The maximum angle for which the scattered light will interfere with the transmitted plane wave is:

$$\cos\theta = 1 - \frac{c\tau}{z}, \tag{2.26}$$

where c is the speed of light and τ is the duration of the pulse. Assuming the duration of the pulse is much shorter than the travel time from the object to the detector ($c\tau << z$), the angle becomes:

$$\sin\theta = \sqrt{\frac{2c\tau}{z}} = NA_{pulsed}. \tag{2.27}$$

The effective numerical aperture will be the smaller of equations 2.25 and 2.27. For very short pulses (<100 femtoseconds) the coupling between temporal and spatial resolution can become a limiting factor, and it might require the use of optical magnification to achieve high resolution. The object can be magnified using a 4-F system (Fig. 2.9b) such that the object field is reproduced in the output plane with a magnification given by $M = f_2/f_1$. The advantage of using a 4-F system is that at the output of the system the reference will still be a plane wave. The effect of magnifying the object field is equivalent to reducing the curvature of the wavefront at the detector, thus reducing the difference in the arrival time between object and reference light fields. The maximum resolution that can be obtained for a given pulse duration is:

$$\delta_t = 0.61 \frac{\lambda}{NA_{pulsed}} \frac{1}{M} = 0.61 \sqrt{\frac{z}{2c\tau}} \frac{\lambda}{M}. \tag{2.28}$$

However, the requirement of having an object that is small relative to the recording area may impose a limit on the desired magnification. As a result, the object size, the magnification and the pulse duration all need to be considered in order to achieve the optimal design for a given application. We have found that for capturing the small filaments generated when the optical beam breaks up due to the nonlinear effects, a magnification of $M = 12$ provided good spatial resolution without compromising the accuracy of the reconstruction.

For the experiments with single frame capture, the numerical aperture of the 4-F system is $NA = 0.25$, the magnification is $M = 12$, $z = 300$ mm, $\lambda = 800$ nm, $\tau = 150$ femtoseconds and the size of the hologram is 10 mm x 10 mm. The resolution limit due to the pulse duration becomes $\delta_t = 2.3$ μm, while the resolution limit due to the numerical aperture is $\delta_H = 2.4$ μm. We are close to an optimum point where we are at the limit of both spatial and temporal resolution. Beyond this point, we would have to sacrifice temporal resolution to improve the spatial resolution, and vice versa. With this setup we have experimentally measured features as small as 4 μm (see Chapter 2). For the experimental parameters used for the multiple frame capture (described in the next section), recording distance $z = 200$ mm and unit magnification ($M = 1$), the resolution limit imposed by the pulse duration is δ_t

= 23 μm. For the same parameters, and a hologram size of 5 mm x 5 mm (only a fraction of the CCD sensor area is used for each hologram), the resolution limit due to the *NA* of the hologram is δ_H = 39 μm; therefore in this case the pulse duration is not the limiting factor. However, for τ < 52 femtoseconds, the pulse duration would become the limiting factor. In this chapter we have covered issues specific to on-axis recording; for a general discussion of the problem of image recovery in off-axis holography with ultrashort pulses see the discussion in Leith et al. [17].

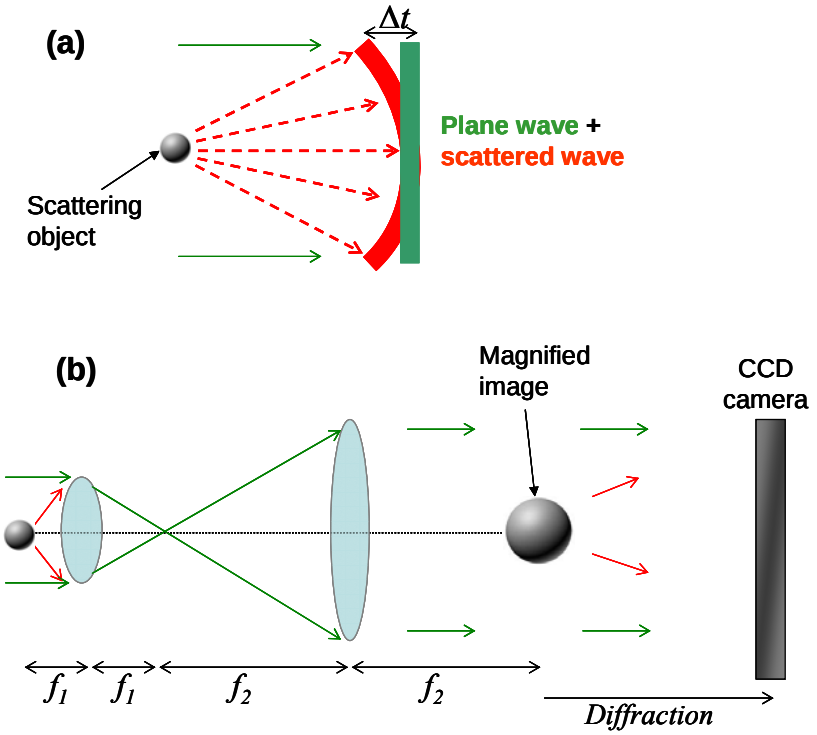

Figure 2.9. Resolution limit. (a) Coupling between temporal and spatial resolution. The time of arrival at the CCD sensor depends on the scattering angle. (b) The resolution can be improved by using a 4-F imaging system to magnify the object.

REFERENCES

[1] D. Gabor, Nature **161**, 777 (1948).

[2] H. J. Kreuzer, M. J. Jericho, I. A. Meinertzhagen, et al., Journal of Physics-Condensed Matter **13**, 10729 (2001).

[3] Z. W. Liu, G. J. Steckman, and D. Psaltis, Applied Physics Letters **80**, 731 (2002).

[4] S. Schedin, G. Pedrini, H. J. Tiziani, et al., Applied Optics **40**, 100 (2001).

[5] R. Boyd, *Nonlinear optics* (Academic Press, San Diego, 2003).

[6] G. P. Agrawal, *Nonlinear fiber optics* (Academic Press, San Diego, 1995).

[7] C. W. Dirk, W. C. Herndon, F. Cervanteslee, et al., Journal of the American Chemical Society **117**, 2214 (1995).

[8] A. Braun, G. Korn, X. Liu, et al., Optics Letters **20**, 73 (1995).

[9] A. Couairon, S. Tzortzakis, L. Berge, et al., Journal of the Optical Society of America B-Optical Physics **19**, 1117 (2002).

[10] A. Piekara, IEEE Journal of Quantum Electronics **QE 2**, 249 (1966).

[11] J. Goodman, *Fourier Optics* (McGraw-Hill, New York, 1996).

[12] G. Liu and P. D. Scott, Journal of the Optical Society of America A-Optics Image Science and Vision **4**, 159 (1987).

[13] M. H. Maleki and A. J. Devaney, Optical Engineering **33**, 3243 (1994).

[14] R. Gerchberg and W. O. Saxton, Optik **35**, 237 (1972).

[15] Y. Zhang, G. Pedrini, W. Osten, et al., Applied Optics **42**, 6452 (2003).

[16] V. V. Volkov and Y. M. Zhu, Optics Letters **28**, 2156 (2003).

[17] E. N. Leith, P. A. Lyon, and H. Chen, Journal of the Optical Society of America A-Optics Image Science and Vision **8**, 1014 (1991).